

Directly Imaged Exoplanets

– Exoplanets A: Final Assignment –

L. Welzel¹, R. van Gaalen¹, J.A. Barendse¹, O.B. Swida¹

Leiden University,
e-mail: welzel@strw.leidenuniv.nl

Submitted May 18, 2023

1. Introduction

Since the inception a few decades ago, exoplanetary study keeps growing and getting more sophisticated with the current technology that we have today. One of the key steps in exoplanet observation is determining whether a star system has an exoplanet or not. Therefore a sky survey is utilized to get a list of potential objects across the sky. Possible exoplanets or planetary system are flagged as *Object of Interest*. Some notable sky surveys that do research on exoplanets are ASTEP South (Crouzet et al. 2010), Kepler (Thompson et al. 2018), and TESS (Sullivan et al. 2015) that uses different techniques and methods to gather their data.

There are different kinds of sky survey methods that we can use, for example:

- **Direct imaging survey:** where we take an image from a relatively small number of stars and check whether they might host exoplanets.
- **Transiting exoplanets:** where we determine the existence of exoplanets around a star based on the star's photometric behaviour.
- **Modelling and statistics:** where we model the star's characteristic in a patch of sky and then use it to estimate the number of stars hosting exoplanetary systems. Currently this method is not reliable since it depends on so many external factors like the Sun and Moon altitude in the observation site (Crouzet et al. 2010).

Sky surveys hold some very important functions in the field of exoplanet research, some of them are (Lagrange 2014):

1. Find more Earth-like planets in the universe that might be capable of incubating intelligent life.
2. Broaden our understanding of the universe, including how planets (especially giant planets) form and evolve over their life time.
3. Broaden the understanding of planetary system diversity. We might find diverse planetary conditions (such as their orbital and physical characteristics) in the universe that we didn't know was possible.

Direct imaging is a powerful technique used in the field of exoplanet research to detect and study exoplanets by directly imaging their light. Unlike other detection methods, such as transit and radial velocity surveys, direct imaging allows astronomers to directly observe exoplanets and their atmospheres. This provides unique insights into their physical properties, such as mass, size, and composition. With direct imaging, astronomers can study a wider range of exoplanets, especially those that are far from their host stars and those that have long orbital periods.

While direct imaging is a challenging technique that requires advanced instrumentation and sophisticated data analysis, it also requires some particular conditions in the system to be observable. Some requirements for direct imaging exoplanets are¹:

1. A planet should have a large semi-major axis; $a \gtrsim 20AU$
2. A planet should have a large enough radius to provide a luminosity $L_{planet} \gtrsim 10^{-10}L_*$

Recent technological advancements have made it possible to detect and study a growing number of exoplanets using this method. As such, direct imaging is an important tool for advancing our understanding of exoplanetary systems.

In this paper we will dive deep into the observations of exoplanets using the **Direct Imaging** method. In section 2 give a detailed description on how Direct Imaging works, after which we present direct imaging detections and interpret these results based on Directly Imaged Planet (DIP) models in section 3. Then in section 4 we give a short discussion of key results and give an overview of the future of this field and High-Contrast Imaging (HCI).

¹ These are approximations and not strict requirements. The exact value might vary for each star system

2. Methods

2.1. Instruments

Direct imaging of exoplanets might be the application with the tightest constraints on instrument design. With the contrast between planet and host-star exceeding a factor of 10^6 , there are only a few instruments that are up for the task. Most detections were performed using the SPHERE instrument at the VLT (Beuzit et al. 2019) and GPI at the Gemini Observatory (Macintosh et al. 2014). These instruments are quite similar and both contain the necessary components for high contrast imaging through angular-, spectral-, and polarimetric differential imaging. The most important of these is the apodizer; usually in the form of a Classical Lyot coronagraph (2.1.1). Other important factors that we will touch on are adaptive optics (2.1.2), polarimetry (2.2) and angular- and spectral differential imaging 2.5.

2.1.1. Coronagraphs/Apodizers

After about a decade of direct imaging, the number of different apodizers is quite large. The most popular is still the classical Lyot (Lyot 1939). It consists of 2 masks to block the source centered in the field. One of these masks is an occulting spot, which contains an absorbing material in the center and transmits light everywhere else, and is located in the focal plane. This blocks most of the starlight, but diffraction still lets light pass an occulting spot larger than the source. This is where the lyot stop comes in; this mask is located in the pupil plane and narrows the beam diameter. This mask cleans up the point-spread function (PSF) of the star, but as it is in the pupil plane the same will happen to the planet's PSF which means we lose some science photons. As it is light from the outer rings (of the star's PSF) in the airy pattern that is filtered, and the planets PSF lies underneath one of these outer rings, this mask still yields a net improvement. Both SPHERE and GPI feature a number of these coronagraphs, with different diameters for the pupil mask to suit sources with different apparent angular sizes (Beuzit et al. 2019; Macintosh et al. 2014). SPHERE also features a Four Quadrant Phase Mask (4QPM) coronagraph which also consists of a focal- and pupil-plane mask, but the focal plane mask doesn't block any light. It is divided up into 4 sections, 2 of which shift the phase of all the light that passes through it by 180° . This leads to destructive interference of the Airy disk on the detector. SPHERE features an achromatic 4QPM, which features four quadrants each with half-phase plates, which shift the phase by only 90° . The fast axis of two of the quadrants is rotated by 90° in order to still achieve the destructive interference (Carlotti, A. 2013). JWST, which has recently performed the first direct imaging observations, features classical Lyots as well. Some of these feature a slanted bar shape in the focal plane occulters as this allows many different

inner working angles without the additional moving parts a higher number of masks would require. The MIRI instrument also features 3 4QPM's (Boccaletti, A. et al. 2022). Despite 4QPM's working well for sources with different apparent sizes, it still needs 3 different masks as the half-waveplates this mask consists of are inherently chromatic.

2.1.2. Adaptive Optics

Apodizers are a great way of increasing the contrast between a star and its companion, but as we do not want to cover the exoplanet, we make the occulting spot as small as possible. This does mean, though, that any movement of the source leads to a large leak of starlight. Although astronomical sources move very predictably, atmospheric interference leads to small but erratic movements. We can counteract this using an Adaptive Optics (AO) system. An AO system features an additional detector, which is called the wave-front sensor (WFS). There are a number of types, of which the Shack-Hartmann is the most popular. This type is also used in SPHERE and GPI (Beuzit et al. 2019; Macintosh et al. 2014). A Shack-Hartmann WFS has a lenslet array in front of the detector. This is a set of lenses that each focus the light of a subsection of the beam onto the detector. As we can then consider parts of the beam separately we can derive the wavefront error up to the same scale as the size of these lenses. We then convert the error into a correction with which is then applied to one of the mirrors. This is possible through the use of deformable mirrors. Deformable mirrors consist of either a number of piston actuators with a flexible reflective surface laid on top, or a piezo system which has a small mirror segment on top of each actuator (which then include some rotational movement as well). Modern AO systems consist of multiple correcting mirrors. The addition of a tip/tilt mirror offers an improvement as it can offload the first order corrections from the deformable mirror. Corrections of the first order require a lot of travel and therefore need a fast moving mirror, while the amount of actuators the higher order corrections require prevent this. The easiest solution is then to separate these functions into separate mirrors. Some systems go a step further and include two deformable mirrors; one for lower order and one for higher order corrections, but as these differ only in the amount of actuators. Introducing more correcting mirrors does make the system very computationally expensive, as the correction needs to be determined from the wave-front error and this correction then has to be divided efficiently over the mirrors. This whole process also has to happen a factor 10 faster than the variation in the wavefront error (Keller et al. 2015).

2.1.3. Interferometers

Using Apodizers has been effective in increasing the contrast between the star and its companion and there have been plenty of successful detections using this

technique only, but we can do more. By only using a coronagraph we do not make use of what we already know about these companions. We will see in section 2.2 that anisotropies we expect in planets, but not in stars lead to differences in the polarization of the light originating from these sources. Furthermore we know that there are significant differences in chemical abundances between this type of planet and the host stars, which means we can subtract a normalized image in a filter the star is bright in from our science image get an image of the exoplanet. These two techniques can work by taking two images, one in each polarization/filter, but this requires a CCD with a high amount of contrast as it does still need to record both the star and planets signal. This is where interferometers come in. By combining the beams on the detector with a half wavelength delay, we introduce destructive interference. This means we get our final image on the detector itself, removing the need for a detector with $10^6 - 10^{10}$ dynamic range.

2.2. Polarimetry

Light with a preferential EM oscillation direction is said to be polarized and can be described with the Stokes vector \mathcal{S} , Equation 1. Light can be polarized by reflection/scattering, including thermal photons from exoplanets that pass through its atmosphere and scatter off of dust. (van Holstein 2021) Since the planet is unresolved in HCI, its net linear polarization is zero if it is uniform, however can be between 0.1 – 2.5% if there are asymmetries such as clouds (Marley et al. 2013), storms/particulates (Karalidi et al. 2013), obscuring companions Sengupta et al. (2016) or a circumsubstellar disk (Stolk et al. 2017). Scattered light from the (mainly unpolarized) star is also polarized (Zugger et al. 2010; Karalidi et al. 2012).

$$\begin{aligned} P &= \frac{PI_L}{I} = \frac{\sqrt{Q^2+U^2}}{I}, \text{ with } \mathcal{S} = [I \ Q \ U \ V]^T \\ \chi &= \frac{1}{2} \arctan\left(\frac{U}{Q}\right) \end{aligned} \quad (1)$$

with total flux I , the linear polarization intensities Q, U , and V the circular polarization intensity, see also Fig. 2 in Van Holstein et al. (2016), and PI_L the linear polarization intensity, P its degree, and χ its angle. (Mansuripur 2002)

2.3. Astrometry

Astrometry finds the (relative, projected) trajectory of a planet about its host star by imaging its position over time. The thermal emission of the planet is imaged using HCI over a period of time and its orbit is fit to it. (Sahlmann et al. 2016; Bruna et al. 2023) Recently, there has been effort to combine different observation techniques to obtain better fits and break degeneracies, highlighting the importance of astrometry for investigating exoplanets. (Lacour et al. 2019; Bruna et al. 2023) Currently, there are efforts

to search for companions of young earth-like stars in the Young Suns Exoplanet Survey (YSES, Kenworthy et al. (2021)) where the astrometric measurements seem to challenge current planet formation and migration theories, see also section 4.2. (Bohn et al. 2020b,a, 2022; Wagner et al. 2022)

2.4. Disk Kinematics & Dust Trapping

Circumstellar disks can be directly imaged and exoplanets leave traces that can be detectable in the disk structure (Andrews 2020; Jorquera et al. 2021) even if the (proto-) planet itself is unresolved (Pinte et al. 2023). This also applies to the imprint of migrating planets (Meru et al. 2019; Welzel 2021) and high eccentricity and/or separation planets which leave imprints in the disk, however finding the trajectory of the latter is made difficult by a number of degeneracies (Nguyen et al. 2020; Rodet et al. 2022).

Dust trapping is the process of dust accumulating around the libration points of the planet-star system, while potentially trapped dust has been imaged using ALMA not confirmed exoplanet has been found using this method to our knowledge (Fedele et al. (2017)², see also the simulated images in Pérez et al. (2019)).

2.5. Differential Imaging

Differential imaging includes several methods that make use of a number of images taken at different telescope orientations section 2.5.2, wavelength windows section 2.5.1 or make use of a reference star to reduce (speckle) noise and contrast. The latter technique makes use of the PSF of a reference star without (known) companion to remove the stellar flux (RDI, Lafrenière et al. (2009)) and is often combined with the other techniques, see section 2.5.3.

2.5.1. Spectral Differential Imaging

Spectral Differential Imaging (SDI) makes use of the different spectra and thus flux at specific wavelengths of host star and companion as well as PSF wavelength scaling to reduce speckle noise. (Smith 1987; Biller et al. 2007).

2.5.2. Angular Differential Imaging

For Angular Differential Imaging (ADI) the telescope is rotated about its observation axis³ between imaging the system. As static speckle noise rotates with the telescope but the exosystem does not, the contrast can be improved by derotating the images and taking a median through the image cube. (Marois et al. 2006)

² However, there is a recent potential confirmation by Hammond et al. (2023) and Currie et al. (2022b).

³ Its a bit more complicated than that for ground observatories as we need to wait for the earth to rotate but that is the basic idea.

2.5.3. Combinations

Often, differential imaging methods are combined to reduce speckle noise (Vigan et al. 2010; Kiefer et al. 2021) or are combined with other HCI methods (Van Holstein et al. 2017). Typically, specific these methods are also combined with other statistical methods for data reduction as primary component analysis, and local noise suppression like LOCI (Marois et al. 2010a).

2.6. Molecular Mapping

Molecule⁴ mapping (Hoeijmakers et al. 2018) is a recently introduced powerful direct imaging technique in that is more powerful at small separations where residual speckles from DI are strongest. The spectrum at each spacial pixel in the 4D spectral image cube is cross-correlated with known spectra of molecule species (or mixtures thereof) over a range of velocity shifts. The result is a maximum cross correlation for each spacial pixel which corresponds to the likelihood of the molecule species detection at a specific velocity shift. With the only input being the spectra of probed species the method thus produces planet and molecule species (non)detection as well as velocity shifts but requires moderate-high resolution direct spectra.

2.7. Modeling

Through direct imaging we can learn a lot more about a planet than other detection methods allow. As we detect photons from the planet itself, we can even study complex atmosphere dynamics. This is not straightforward though. As we can only directly detect compound abundances, we need atmosphere models in order to make sense of the processes that are going on. One of such models is Exo-REM (Baudino et al. 2015), as inputs it takes the planet's surface gravity, effective temperature, and elemental composition. By modeling the evolution until it finds a stable state, it can determine the temperature profile, abundances at different radii, and a spectrum (for self-consistency). Despite the continuous improvements made to these models, we can not match the complexity of atmospheres. This is a significant constraint on our understanding of planet interiors. They are almost exclusively 1D and only incorporate a small amount of chemical compounds and reactions. Furthermore the assumption that the atmosphere is in chemical- and thermal equilibrium usually does not hold. Processes like vertical mixing, photo-chemistry, clouds, and/or atmospheric escape can cause this.

2.8. Verification & Characterization

Once we have the list object of interest, we can use the methods aforementioned in section 2 to determine whether these objects are exoplanets or background/foreground noise detected as false positives.

⁴ Sometimes also molecular mapping.

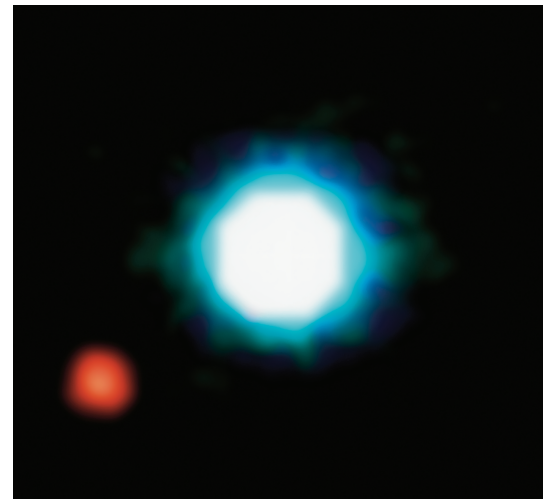


Fig. 1. First direct imaging observation. The brown dwarf 2M1207 (middle) and the exoplanet 2M1207 b (red) are 230 light-years away, in the constellation of Hydra. The photo is based on three near-infrared exposures (in the H, K and L wavebands) with the NACO adaptive-optics facility at the 8.2-m VLT Yepun telescope at the ESO Paranal Observatory. Credits: NASA (2023)

Exoplanet verification and characterization are crucial steps in the study of exoplanets and involve confirming the existence of exoplanets and determining their physical and orbital properties. One example on the usage of verification and characterization is using the astrometry (Perryman et al. 2014) to observe the movement of a light source (planets, brown dwarf, or other object of interest) around a star.

Although we have already suspected the existence of detectable direct imaging exoplanet for a long time (Michel Mayor 1995), the technology was only available not more than 2 decades ago. The first ever direct imaging of an exoplanet was only made in 2004, made by ESO's Very Large Telescope (NASA 2023) shown in Figure 1.

The main challenge in detecting exoplanets using direct imaging technique is how to differentiate the signal (exoplanets) from noise. Using method developed by Perryman et al. (2014), we can conclude that an object of interest (an exoplanet) can be confidently⁵ detectable if they have Signal-to-Noise bigger than the detection threshold.

$$S/N \equiv \frac{\alpha}{\sigma_{\omega}} > n \quad (2)$$

Where n is detection threshold in range $n = 0.5 - 6$ based on the star system, α is astrometry signature, and σ_{ω} is sky-average parallax accuracy. This resulting for GAIA to be able to detect 20.000 - 30.000 exoplanets around G-stars with the mass of $M_{planet} \leq 15M_{Jup}$.

In recent years, there have been significant advances in the field of exoplanet characterization, with new techniques such as transmission and emission spectroscopy (de Kok et al. 2013), atmospheric mod-

⁵ The parameters can be adjusted but it affect the accuracy

eling (Stevenson et al. 2014), and machine learning methods being developed to extract as much information as possible from the limited data available for most exoplanets (Marquez-Neila et al. 2018).

3. Results

3.1. Population

Unlike most of the exoplanets discovered by alternative methods, Directly Imaged Planets or DIPs have wide orbits ($\sim 10\text{-}250$ AU) and are at least 2 times more massive than Jupiter. Most are young, self-luminous gas giants, some are even still protoplanets or have just passed this phase Currie et al. (2022a).

Before discussing the population of DIPs, we first need to mention no clear agreement exists on the definition of a planet. Some of the direct imaged objects could also be interpreted as brown dwarfs. That is, the deuterium-burning limit is $13M_J$, but the accretion of gas does not necessarily shuts off when this mass is reached. Studies into the definition of brown dwarfs also look into the semi-major axis of the orbit and the mass ratio relative to the host-star. The semi-major axis of planets is unlikely to exceed 300 AU, due to typical size of disks in which planets form Andrews et al. (2007). A few of the observed direct imaged objects exceed either a 300 AU separation from its host star or the deuterium-burning limited mass of $13M_J$. That explains the difference in number of DIPs mentioned by the NASA Exoplanet Archive (2023) which states 49 planets and by the NASA Exoplanet Exploration Program (2023) which states 64 planets.

While Currie et al. (2022a) gives semi-major-axes of 10–250 AU, Currie et al. (2022b) states 50–300 AU and Macintosh et al. (2015) provides a range of 9–650 AU. This huge difference on the maximum semi-major-axis is mostly influenced by the definition of planets. The minimum separation is in principle only be limited by our observation techniques.

3.1.1. Stars

Besides the population of direct imaged exoplanets, it is interesting to look into the population of host-stars they orbit. According to Currie et al. (2022a), most of the host-stars are B, A, or F stars (all at least 50% more massive than the sun), and have typical ages of 10–100 Myr. The majority of these stars are part of young nearby stellar associations. Most of these systems also have debris disks like the Kuiper belt.

3.1.2. Orbits

Due to their wide separations from their host-star, DIPs typically have long orbital periods ($\sim 10^1 - 10^5$ yrs), which challenges determining reliable constraints on these periods, as well as on other orbital properties such as eccentricity and inclination.

The occurrence rate of planets at large separation is relatively high, which could be an indication that

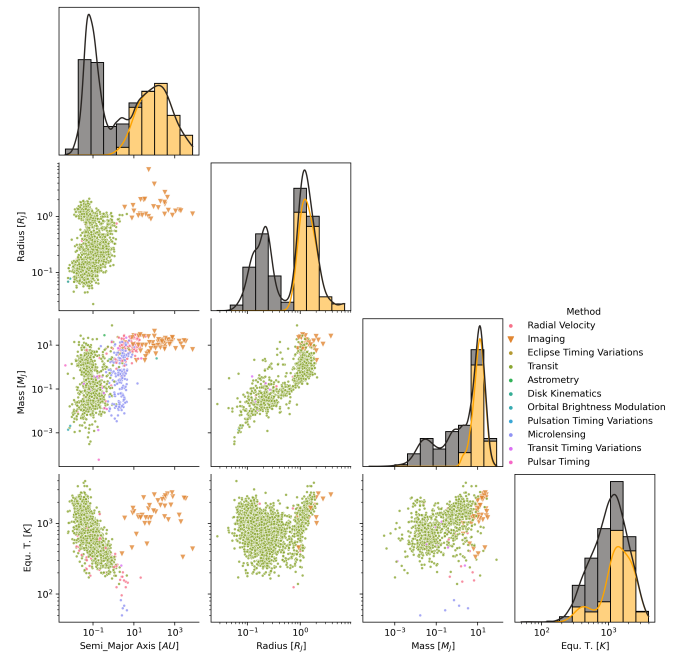


Fig. 2. The known semi-major-axis, mass, radius and T_{eq} for the full exoplanet population are shown relative to each other, where the detection method is indicated for each planet. It can be clearly seen that the properties of DIPs cover another range than the properties of non-DIPs. The densities of the planets however follow a similar distribution. The mass distribution, as well as the T_{eq} distribution of DIPs is shifted to higher values compared to other detection methods. The four bar plots show the distribution of planets detected by a certain detection method (where for each plot the x-axis is binned into 10 bins). The data used to produce this plot is from NASA Exoplanet Archive (2023). This data may contain brown-dwarfs or protoplanets, as NASA included some objects that are not included by other sources.

the orbits of these planets have been highly influenced in the past (Kenworthy 2023).

Some C/O ratios found in the DIPs are solar-like, which suggests these planets are formed in regions with high metallicity and close to their host-star, and migrated outwards after their formation (see section 3.2). One of these planets is β Pic b, which will be discussed in section 3.3.3.

3.2. Atmospheres

The major advantage direct imaging of exoplanets has over other methods is that it uses photons originating in the planet itself or scattered by its atmosphere or surface. This means that for young (up to 200–300 Myr, Currie et al. (2022a) and Ruffio et al. (2023) respectively depending on instrument, separation etc.) Jovians we can probe and map the atmosphere separate from the host star. In the following we will be careful to constrain the consideration to planets, even though there is overlap and uncertainty about the separation between them and brown dwarfs and our understanding of DIP is significantly informed by brown dwarfs (L, T type) (Currie et al. 2022a).

3.2.1. Composition

For most DIPs, a distinguishing feature in their atmospheres is molecule formation, specifically complex molecules such as Methane (CH_4), and the suspected presence of sub μm dust and hazes. (Deming et al. 2017; Madhusudhan 2019)

Direct imaging often has high spectral resolution and is combined with other spectroscopic measurements. Noteworthy is that different wavelengths probe different layers in the atmosphere of DIP, depending on their composition and (dynamic) structure. (Bur-gasser 2009; Currie et al. 2022a)

The atmosphere is characterized using a number molecular tracers which have characteristic lines in the spectral window of the instrument. The most impact tracers are H_2O , CO, CO_2 and CH_4 . (Lee et al. 2013; Madhusudhan 2019) Recently there has been a heightened interest in sulfur-species such as H_2S (Polman et al. 2022) and nitrogen species such as N_2 , NH_3 and HCN (Moses et al. 2016) as well as more carbon species such as C_2H_2 (Rimmer et al. 2014; Moses et al. 2016). In the near future especially nitrogen bearing species will see more attention and N/O (potentially also S/O) might complement C/O ratios as an important formation and composition tracer (Danielski et al. 2018; Patapis et al. 2022). This is because the H–C–O–N system strongly influences the atmosphere, especially of colder < 600 K exoplanets such as GJ 504 b and future targets (Woitke et al. 2021). Phosphine, alkali metals such as Na, K, Mg & I as well as Ti-, Al- and Li-compounds, Ca and Fe are also important for dust, cloud and haze formation (Gao et al. 2021; Kempton et al. 2017) and refractory species Madhusudhan (2019). The composition of DIP is strongly related to their protoplanetary disk, with budgets comparable to those in Figure 3 c).

Recently, Miles et al. (2023) published the a new high resolution $1 - 18\mu\text{m}$ spectrum of VHS 1256 b as part of the JWST ERS, showing rich spectral features at high resolutions. While caution is advisable when interpreting ERS spectra we highlight that while Miles et al. (2023) report a "significant" silicate cloud feature, they currently do not find evidence for species (C_2H_2 , C_2H_4 , C_2H_6 , H_2S , PH_3 & HCN) which would be expected from disequilibrium chemistry.

The C/O ratio of a planet, star, disk, or cloud is a key tracer for atmospheric composition and chemistry. It also tentatively indicates where in the circumstellar disk the planet has formed and if the planets atmosphere originates from its birth-place in the disk or if it was accreted at later times or while migrating. This is because the protoplanet is typically thought of forming in a specific region of the disk, where the local conditions differ from the overall composition. The main differentiating features are snowlines of volatile carriers, O, C and N which sequentially freeze-out as the distance to the star increases, and hence stellar flux and temperature decrease, see Figure 3 but note that the N/O ratio in gas/solids is sub-

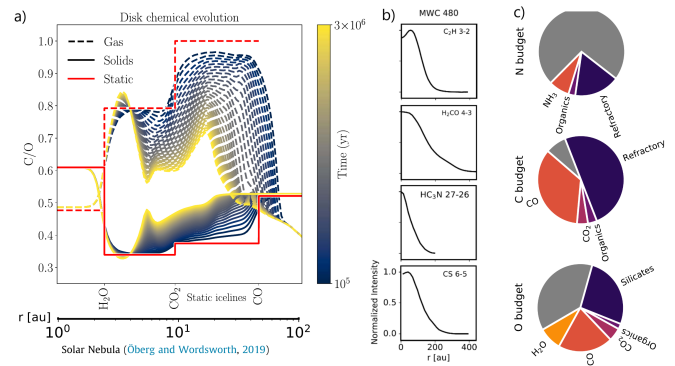


Fig. 3. C/O ratios and molecular composition of protoplanetary disks. a) The C/O ratio in gas and solids as a function of radius for protoplanetary nebula and the evolution of this ratio over time as well as the ice lines for H_2O , CO_2 and CO (Mollière et al. 2022), the second axis gives the approximate scale for the solar protoplanetary disk, b) The normalized abundances of selected molecules in MWC 480 as a function of radius (Öberg et al. 2021), and c) the budgets of oxygen, carbon and nitrogen in protoplanetary disks, gray indicates unknown species, however much of the gray slice for N_2 is probably N_2 (Öberg et al. 2021).

stantially different from C/O (Öberg et al. 2021) and thus C/O+N/O jointly better constrain formation than each individually.

Comparing the C/O ratios in the disk in Figure 3 with the measure ratios for the DIP in Figure 4 we can see that most planets must have formed inside of the CO_2 iceline. This is because outside of this ice-line carbon and oxygen are most abundant in CO gas which leads to $\text{C}/\text{O} = 1$ Madhusudhan (2019). Note-worthy is 51 Eri b which has a C/O ratio of ~ 0.9 but is also far inside the CO_2 iceline for 51 Eridani (F0IV, 10–20 Myr, Brown-Sevilla et al. (2022)). This means that the formation history of 51 Eri b is inconsistent with the current model from which we would expect a much lower C/O ratio, especially when considering the evolution of the C/O ratio for gas from Figure 3 a). Still, there is strong disagreement about the actual C/O ratio of 51 Eri b which needs new observations to be resolved, compare the C/O results from Brown-Sevilla et al. (2022) and Wang et al. (2022). The other planets are consistent with formation in the inner system and outwards migration. AB Pic b is at especially large separations, however its C/O ratio is close to what would be expected for moderate migration. This has two potential explanations, either the planet migrated late through a partially depleted disk, again see the evolution in Figure 3 a) or accumulated large amounts of oxygen species initially which balance the later carbon rich accretion (see C-species abundance in Figure 3 b). This highlights that a wide range of C/O ratios is explicable with different migration histories and future observations of N/O ratios as well as other tracer species together with disk modelling will refine our understanding of the composition of DIP.

3.2.2. Chemistry

The atmospheres of the DIP are probably vertically well mixed on timescales much smaller than required

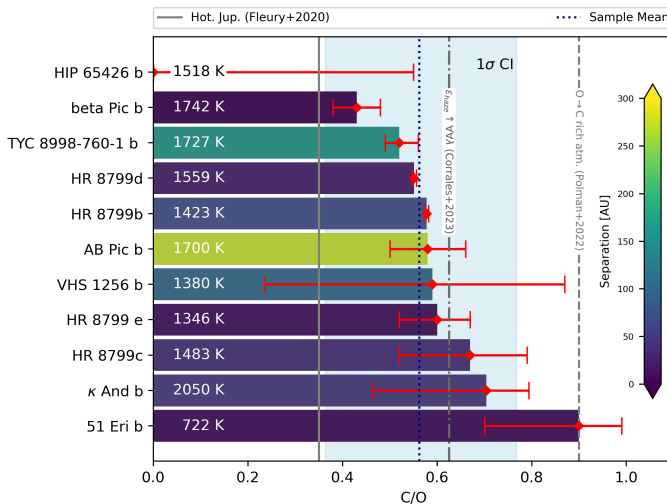


Fig. 4. C/O ratio of confirmed, fully formed directly imaged exoplanets ($< 13M_J$ at 1σ) with known C/O ratios or upper limits. The mean C/O ratio of the sample is slightly supersolar ($C/O_{\odot} \approx 0.5$, Madhusudhan (2012)) and just below the C/O ratio where absorptivity ε at almost all wavelengths sharply rises due to strong hazes for planets with $T_{atm} < 800K$ (Corrales et al. 2023). For planets with $1250 < T_{eff} < 1700 K$ the atmosphere starts to transition from oxygen to carbon rich at $C/O \sim 0.9$ which should produce a clear transition in the observed spectrum as H_2S is obscured by HCN and C_2H_2 (Polman et al. (2022) at $Z \sim 10Z_{\odot}$, mostly concerned with the transmission spectrum). Note however, that these ratios are also a function of T, g, Z, \dots . Indicated is also $C/O = 0.35$ since Fleury et al. (2020) performed laboratory experiments on the chemistry of hot Jupiter sample atmospheres at this ratio and unity. The significant outliers are HIP 65426 b for which only an upper limit is known and 51 Eri b, which is much colder than the other planets. Data from (each entry as; Planet: direct imaging reference & C/O references & T_{eff}) HIP 65426 b: Chauvin et al. (2017) & Petrus et al. (2021) & Petrus et al. (2021), beta Pic b: Lagrange et al. (2010) & Nowak et al. (2020b,a) & Nowak et al. (2020b,a), TYC 8998-760-1 b: Bohn et al. (2020a) & Zhang et al. (2021) & Bohn et al. (2021), HR 8799d: Marois et al. (2008) & Ruffio et al. (2021); Wang et al. (2021) & Wang et al. (2021), HR 8799b: Marois et al. (2008) & Ruffio et al. (2021) & Wang et al. (2021) (in stark contrast to Lee et al. (2013)), AB Pic b: Carson et al. (2013) & Palma-Bifani et al. (2022) & Palma-Bifani et al. (2022), VHS 1256 b: Stone et al. (2016) & Hoch et al. (2022); Hoch (2022a); Miles et al. (2022) & Petrus et al. (2023), HR 8799 e: Marois et al. (2010b) & Mollière et al. (2020) & Wang et al. (2021), HR 8799c: Marois et al. (2008) & Wang et al. (2020); Ruffio et al. (2021); Wang et al. (2022) & Wang et al. (2021), κ And b: Carson et al. (2013) & Hoch et al. (2020) & Hoch (2022b), 51 Eri b: Macintosh et al. (2015) & Whiteford et al. (2023) & Whiteford et al. (2023). We do not report the data for GJ 504 b (Skemer et al. 2016) due to the limitations of the C/O estimate of ($C/O = 0.20^{+0.09}_{-0.06}, T_{eff} = 544 K$) by Bonnefoy et al. (2018) (discussed therein) and its mass (Danielski et al. 2018), nevertheless we note that this estimate, similar to the planets temperature, is exceptionally low. If references disagree the higher S/N and then the more recent one was given preference. This is the first such overview to our knowledge, though naturally there exist many C/O relations for exoplanets and brown dwarfs.

for equilibrium chemistry, see section 3.2.3 and section 3.2.4. This is further supported by the absence of CH₄ surface features in the many of the atmospheres, which differentiates the DIP strongly from most brown dwarfs. Note though that there is evidence for deep methane absorption (L-band) in several DIP (Miles et al. 2018). Together this implies non-equilibrium CO \leftrightarrow CH₄ chemistry which in turn

relates to high variability caused by clouds and short lived clear patches, see section 3.2.4. (Skemer et al. 2014; Miles et al. 2018) Theoretically, the disequilibrium chemistry has been predicted based on Jupiter, where chemical quenching dominates the atmosphere compositions. Quenching is likely also a strong driver for upper atmosphere composition in DIP, as their T-P profiles cross one or both of the CH₄/CO or NH₃/N₂ stability boundaries. The (theoretical and observational) requirement for chemical disequilibrium and vertical mixing has motivated much of the research into vertical eddy mixing and general circulation models (GCM), e.g. by Menou (2019); Mendonça et al. (2018). This non-equilibrium region stretches farther into the interior for colder planets, however, the deep interior high pressure and temperature regions not accessible to us, are almost certainly in chemical equilibrium. (Madhusudhan 2019)

H₂O vapour is the major oxygen reservoir in the atmosphere for all oxygen not bound by CO if the planet is in the CO or the major reservoir if it is in the CH₄ stability region. Only depletes at temperatures lower than inferred for the atmosphere of all DIP. (Madhusudhan 2019)

One major issue with DIP chemistry is the degeneracy between inferred temperature and radius, as current inference methods tend to overestimate⁶ T_{eff} (overestimate flux density) and in turn underestimate the planet's radius which leads to unrealistically (formation theoretic) high core mass $\sim 100M_{\oplus}$, see also section 4.3. (Hoch et al. (2020) and Carrión-González et al. (2020) for reflected starlight)

3.2.3. Structure

Compared to brown dwarfs DIP have a complex structure, mostly due to their lower surface temperature and thus complex molecular chemistry in addition to the H-He dominated atmosphere. The outer envelope is traced by CO, partially by CH₄ gas and might contain some NH₃, NH₄HS and H₂O clouds for the very coldest DIP which obscure the CH₄ gas. Deeper layers are traced by CO with hazes or clouds of refractory species as well as alkali and sulfur species. In the very lowest layers of the atmosphere silicates, oxides and liquid metals might be suspended, with preliminary observational evidence mentioned in section 3.2.1. (Morley et al. 2014; Moses et al. 2016; Sing et al. 2016; Gao et al. 2017; Lavvas et al. 2021) One major impact on the structure of these young DIP are impactors which can mix the atmosphere on large scales, drive local cloud formation on dynamic timescales and are expected to be relatively frequent (maybe $\sim 1/\text{week}$)⁷ for DIP which are partially embedded in disks (Marley et al. 2013; Macintosh 2021).

⁶ While Hoch et al. (2020) addresses this issue the claim is made much clearer in the talks by Macintosh (2021) and Molliere (2021).

⁷ Estimate is by Macintosh (2021), however no specific reference is given.

The considerations in the previous sections concerning clouds and dust lead to higher internal temperatures at a given pressure compared to a brown dwarf since radiative heat loss is less efficient. Inversely, the surface spectrum is also flatter than for a comparable brown dwarf since the surface is covered by large particles emitting in the IR. Directly imaged protoplanet spectra are almost feature-less black bodies. The low incoming stellar flux, evidenced by the absorption features and a lack of stellar emission features, for most of DIP means that no temperature inversions are expected from retrievals. (Madhusudhan 2019)

While there is strong theoretic and observational evidence for clouds and hazes the previously mentioned T-R degeneracy is partially due to observations in the Mid IR probing high clouds or their surfaces and NIR the interior of clouds and Madhusudhan (2019) suggest that solving the degeneracy might require optical observations.

No current observations have the resolution to spatially resolve the surface of DIP, however comparing e.g. 51 Eri b to Jupiter we might expect similarly complex surfaces, with longitudinally and laterally differentiated features. In the future, polarimetry might indicate the presence of such asymmetries. (Marley et al. 2013)

3.2.4. Dynamics

The atmosphere of DIP is likely highly dynamic, with vertical mixing/quenching, impacts and rapid rotation. While the period of brown dwarfs, measured by line broadening, is between 1-30h, the period of DIP is less well constrained, but seems to be between 4-22h. Currie et al. (2022a)

Showman et al. (2013) find that horizontal wind speeds for brown dwarfs and DIP can reach up to 10 – 100 m/s and lead to mechanically driven overturning together with vertically-horizontally coupled vorticity. Since DIP are generally at large separations, with little stellar flux and unlikely to be tidally locked, horizontal chemical quenching would require a different mechanism compared to hot Jupiters. Nevertheless, Showman et al. (2013) expect horizontal movement as stratified zonal jets which couple to the vertical mixing and lead to both large- and small-scale features, bringing up fresh condensate from the interior which freezes out and is advected inwards as dust. These inwards streams will then lack in condensate and thus be visible as "holes" in the cloud cover. At the same time lighter particulates do not settle on convection timescales, might drift on the winds and from a continuous haze layer. A more in-depth analysis is given for brown dwarfs by Tan et al. (2021) and Millar-Blanchaer et al. (2020) report a net polarization for the brown dwarf Luhman 16B and infer surface differentiation.

For DIP fast rotation and differentiated surface features leads to a variability of over 20 – 30% in the NIR (Madhusudhan 2019; Zhou et al. 2022). This variabil-

ity and the expected complex bulk fluid movement drives the development of full 3D GCM to model planets on dynamic time-scales and inform retrievals. (Tan et al. 2021) Nevertheless, relatively low rotational speeds like for VHS 1256 b do not necessarily lead to less variability since these speeds enable larger eddies and thicker clouds. The high variability of DIP supports the image of their atmospheres as highly complex systems that evolve at several timescales and scales both at high altitudes and deeper layers where in-falling matter is re-processed. Currently our image is limited by spatial and spectral quality, however, with future observations local storms might replace zonal waves and spots as the smallest scale phenomena we can infer. (Zhou et al. 2022)

3.3. Examples

This section will further dive into the population of direct imaged exoplanets by exploring a few examples of DIPs. They each have interesting features and together give a general view of the population of DIPs.

3.3.1. HR 8799bcd

The first example is a multiplanet system. That is, the very first DIPs announced are HR8799b, HR8799c and HR8799d, discovered by Marois et al. (2008). They used high-contrast observations from the Keck and Gemini telescopes to detect the three exoplanets at a projected distance from the host-star of 24, 38 and 68 AU. Dynamical models strongly suggest the mass of these planets are $M_{\text{planet}} < 10M_J$. This system is interesting, as it seems to be a scaled-up version from our own solar system Marois et al. (2010b).

3.3.2. 51 Eri b

The planet 51 Eri b is probably the smallest DIP so far, with a radius of $\sim 1R_J$. It is also one of the DIP's that have a clear molecule signature in their atmosphere: Macintosh et al. (2015) found a strong methane signature ($>6\sigma$) in the J-band. The planet orbits at 13 AU from its host star and has a mass in the range 2-12 M_J .

3.3.3. Beta Pic

A well-studied direct imaged exoplanet is β Pictoris b (β Pic b). Compared to the total observed population of direct imaged exoplanets, β Pic b has a small semi-major axis (~ 9 AU), and an orbit of approximately 24 years which has well-known orbital parameters. Its mass is $\sim 9.3M_J$. According to Nowak et al. (2020b), the C/O ratio in the atmosphere is 0.43, which suggests (in combination with the high mass of the planet) a planet formation via core-accretion. This low C/O ratio also is an indicator that the planet could have been closer to the star in the past, and has migrated outwards. The effective temperature of β Pic b is in the range of 1650-1800K.

3.3.4. AB Aurigae

Another interesting direct imaged discovery is a Jupiter-like protoplanet at a approximately 93 AU projected separation from its host star AB Aurigae, found by Currie et al. (2022b). This system is a key to understand planet formation at wide separations. The core accretion model —where the core of gas giants is slowly but steadily increasing over time, after which an envelope is rapidly accreted— is the widely accepted theory about the formation of our own solar system giants. However for large separations and high-mass exoplanets, a more plausible explanation is disk instability, where planet forms via gravitational collapse (Boss 1998). The angular separation of AB Aurigae b with its host star is 0.59". The hill radius of the planet is spatially resolved and approximately 7 AU. In the best-fit model, the planet has a mass of $9M_J$, a radius of $2.75R_J$, an effective temperature of 2200K,

3.4. Far-Out, High Eccentricity or Free Floating Planets?

Recent observations have put renewed focus on wide orbit planets (Bohn et al. 2020b, 2021) as well as initiated prospective surveys (Wide Separation Planets in Time, WiSPiT⁸). These high separation and potentially high eccentricity planets can only realistically be found by direct imaging around young stars. There is tentative indication for relatively high occurrence rates of these high separation planets, however the trustworthiness of this indication is limited by the small number of imaged planets. There is currently no consensus over the history of these planets, however they might offer a look into "failed" free floating planets and strongly constrain planet migration and disk fragmentation. (Miret-Roig 2023; Zhang et al. 2023; Kenworthy 2023)

4. Discussion

4.1. Atmospheres

DIP atmospheres are highly complex, both in structure and chemistry, and dynamic systems that are well understood in principle but poorly understood in detail or on small spatial and temporal scales. DIP atmospheres are a product of their birthplace and evolution in circumstellar disks. Relating disk and planet models offers the potential to fully explain a wide range of phenomena in both fields. Upcoming high resolution spectroscopy and imaging will together cast light on the chemical networks and mechanical processes that produce their beautiful spectra.

4.2. Planet & Star Formation

DIP are a strong constraint on formation and evolution theories of both disks and planets. The high resolution spectra and astrometry data from HCI informs

aspects of solar system evolution inaccessible to other methods. Refined C/O and N/O ratios are a promising avenue for probing the migration of DIP whose direct resolution spectra inform not only their properties but also allows hints at the processes in exoplanet atmospheres at a wide range of altitudes.

4.3. Limits & Bias

As already mentioned in section 1 and section 3.1.2, Direct Imaging needs some strict requirements to be done. This results in limitations in the observations, both physical, observational and technological limitation.

For example, we are currently only able to see objects with angular separations no less than 0.5" (La-grange 2014) otherwise the PSFs of host and companion would be indistinguishable. This would correspond to the detectable planets having $a \geq 5AU$ and in most cases will be $a \gtrsim 15AU$ based on their distance from us.

Also as already mentioned in section 2.8, we are limited to detect exoplanets using direct imaging to a relatively dark patch of the sky with low background noise. This limits our observation to avoid some region of the sky.

Like all detection methods, direct imaging also suffers from a heavy bias. We detect planets with the highest contrast to their host star. This can be achieved by a large semi-major axis and/or large planet mass, so we mainly find large planets that are far out. Figure 2 shows that observations confirm this.

Other bias' that we might encounter is that we more likely to observe relatively young exoplanets compared to older ones. Because we rely heavily on visible or near visible light from the object of interest —in both scattered light from the host and thermal emission— we are favoured towards self-luminous planets, especially those that are close to the detection limits. This might be caused by the physical and thermal activity of the planet itself. While giant planets cool they contract and radiate out their gravitational energy. Therefore young giants are significantly brighter and are therefore favoured (Currie et al. 2022a).

The T-R degeneracy noted in section 3.2.2 strongly impacts cloud model inference and thus needs to be resolved. Recent JWST observations (Miles et al. 2023), see section 3.2.1 might have already resolved this degeneracy for VHS 1256 b using a large frequency window in the IR.

4.4. Future Instruments

Direct imaging detections are still lag behind compared to other methods. Therefore improvements in the instruments could bring new developments to this field. The direction that has received the most attention has been the apodizers. Apodizing Phase Plates (APP) are been used for observations a few times by now. Where conventional apodizers use absorbing materials, APPs are essentially liquid crystals that

⁸ No paper reference; Kenworthy (2023)

have a complex pattern which defines whether light passing through a certain section is retarded. This leads to interference in the focal plane giving the desired PSF. As we want destructive interference at the location where we expect an exoplanet, there is constructive interference elsewhere and the brightness of the star is conserved. This gives us a great reference source, while we still get great contrast within our 'dark hole' (Kenworthy et al. 2007). A APP is, then, essentially a generalized version of a 4QPM. Alignment is no longer important as the same PSF is applied to sources all over the field and as an APP is mounted in the pupil plane, it does not need a lyot stop which gives us higher transmission. One of the drawbacks of APPs is that they are chromatic, but through the use of multi-twist retarder wave-plates this can be mitigated (Komanduri et al. 2013). These so-called vector APPs (vAPP) can offer retardance offsets $<4^\circ$ over more than 2 octaves of spectral range (Snik et al. 2014). The great performance of this type of apodizer is also illustrated by its selection for the METIS instrument on the ELT (Carlomagno et al. 2020). Another direction of improvement could be the use of interferometry. The combination of a vAPP coronagraph with the Large Binocular Telescope Interferometer has recently been demonstrated on sky (Sutliff et al. 2023) and high contrast imaging instruments have also been proposed for the VLTI (Defrère et al. 2018).

5. Conclusion

In conclusion, the study of directly imaged exoplanets has provided unique insights into the physical properties of these objects, particularly their atmospheres and interiors. Direct imaging surveys have allowed astronomers to probe and map the atmosphere of young Jovians separate from their host star, providing valuable information on their composition and dynamics.

Furthermore, direct imaging has enabled the detection of protoplanets together with disks around infant stars, which provides crucial information on the formation of gas giant planets such as Jupiter.

Still, technological limitations still exist in our ability to directly image exoplanets and gather detailed information on their atmospheres and interiors. This causes some biases in our observation and incorrect general conclusion. Continued advancements in technology and methodology are necessary to improve our capabilities in this area.

Overall, the study of directly imaged exoplanets has opened up new avenues for research into planetary science and astrophysics. With further development in technology and methodology, we can expect to gain even more insights into the physical properties of these fascinating objects.

References

- Andrews, S. M. 2020, Annual Review of Astronomy and Astrophysics, 58, 483
 Andrews, S. M. & Williams, J. P. 2007, The Astrophysical Journal, 659, 659
 Baudino, J. L., Bézard, B., Boccaletti, A., et al. 2015, A&A, 582, A83
 Beuzit, J. L., Vigan, A., Mouillet, D., et al. 2019, A&A, 631, A155
 Biller, B. A., Close, L. M., Masciadri, E., et al. 2007, The Astrophysical Journal Supplement Series, 173, 143
 Boccaletti, A., Cossou, C., Baudoz, P., et al. 2022, A&A, 667, A165
 Bohn, A., Kenworthy, M., Ginski, C., et al. 2020a, Monthly Notices of the Royal Astronomical Society, 492, 431
 Bohn, A. J., Ginski, C., Kenworthy, M. A., et al. 2022, Astronomy & Astrophysics, 657, A53
 Bohn, A. J., Ginski, C., Kenworthy, M. A., et al. 2021, Astronomy & Astrophysics, 648, A73
 Bohn, A. J., Kenworthy, M. A., Ginski, C., et al. 2020b, The Astrophysical Journal Letters, 898, L16
 Bonnefoy, M., Perraut, K., Lagrange, A.-M., et al. 2018, Astronomy & Astrophysics, 618, A63
 Boss, A. P. 1998, The Astrophysical Journal
 Brown-Seville, S., Maire, A.-L., Mollière, P., et al. 2022, arXiv preprint arXiv:2211.14330
 Bruna, M., Cowan, N. B., Sheffler, J., et al. 2023, Monthly Notices of the Royal Astronomical Society, 519, 460
 Burgasser, A. J. 2009, arXiv preprint arXiv:0903.1390
 Carlomagno, B., Delacroix, C., Absil, O., et al. 2020, Journal of Astronomical Telescopes, Instruments, and Systems, 6, 035005
 Carlotto, A. 2013, A&A, 551, A10
 Carrión-González, Ó., Muñoz, A. G., Cabrera, J., et al. 2020, Astronomy & Astrophysics, 640, A136
 Carson, J., Thalmann, C., Janson, M., et al. 2013, The Astrophysical Journal Letters, 763, L32
 Chauvin, G., Desidera, S., Lagrange, A.-M., et al. 2017, Astronomy & Astrophysics, 605, L9
 Corrales, L., Gavilan, L., Teal, D., & Kempton, E. M.-R. 2023, arXiv preprint arXiv:2301.01093
 Crouzet, N., Guillot, T., Agabi, A., et al. 2010, A&A, 511, A36
 Currie, T., Biller, B., Lagrange, A.-M., et al. 2022a, arXiv preprint arXiv:2205.05696
 Currie, T., Lawson, K., Schneider, G., et al. 2022b, Nature Astronomy, 6, 751
 Danielski, C., Baudino, J.-L., Lagage, P.-O., et al. 2018, The Astronomical Journal, 156, 276
 de Kok, R. J., Brogi, M., Snellen, I. A. G., et al. 2013, A&A, 554, A82
 Defrère, D., Absil, O., Berger, J.-P., et al. 2018, Experimental Astronomy, 46, 475
 Deming, L. D. & Seager, S. 2017, Journal of Geophysical Research: Planets, 122, 53
 Fedele, D., Carney, M., Hogerheijde, M., et al. 2017, Astronomy & Astrophysics, 600, A72
 Fleury, B., Gudipati, M. S., Henderson, B. L., & Swain, M. 2020, The Astrophysical Journal, 899, 147
 Gao, P., Marley, M. S., Zahnle, K., Robinson, T. D., & Lewis, N. K. 2017, The Astronomical Journal, 153, 139
 Gao, P., Wakeford, H. R., Moran, S. E., & Parmentier, V. 2021, Aerosols in exoplanet atmospheres
 Hammond, I., Christiaens, V., Price, D. J., et al. 2023, Monthly Notices of the Royal Astronomical Society: Letters, slad027
 Hoch, K. K., Konopacky, Q. M., Barman, T. S., et al. 2020, The Astronomical Journal, 160, 207
 Hoch, K. K., Konopacky, Q. M., Theissen, C. A., et al. 2022, arXiv preprint arXiv:2212.04557
 Hoch, K. K. W. 2022a, Moderate Resolution Spectroscopy of Directly Imaged Exoplanets (University of California, San Diego)
 Hoch, K. K. W. 2022b, Moderate Resolution Spectroscopy of Directly Imaged Exoplanets (University of California, San Diego)
 Hoeijmakers, H., Schwarz, H., Snellen, I., et al. 2018, Astronomy & Astrophysics, 617, A144
 Jorquera, S., Pérez, L. M., Chauvin, G., et al. 2021, The Astronomical Journal, 161, 146
 Karalidi, T., Stam, D., & Guirado, D. 2013, Astronomy & Astrophysics, 555, A127
 Karalidi, T., Stam, D., & Hovenier, J. 2012, Astronomy & Astrophysics, 548, A90
 Keller, C. U., Navarro, R., & Brandl, B. R. 2015, Field Guide to Astronomical Instrumentation (SPIE)
 Kempton, E. M.-R., Bean, J. L., & Parmentier, V. 2017, The Astrophysical Journal Letters, 845, L20

- Kenworthy, M. 2023, YSES and WiSPiT: direct imaging surveys for young gas giant exoplanets - Wide Separation Planets in Time, talk at the Artemis Colloquium (2023-03-09), Faculty of Aerospace Engineering, TU Delft. No slides published.
- Kenworthy, M., Bohn, A., Ginski, C., et al. 2021, in European Planetary Science Congress, EPSC2021-35
- Kenworthy, M. A., Codona, J. L., Hinz, P. M., et al. 2007, ApJ, 660, 762
- Kiefer, S., Bohn, A. J., Quanz, S. P., Kenworthy, M., & Stolkér, T. 2021, Astronomy & Astrophysics, 652, A33
- Komanduri, R. K., Lawler, K. F., & Escuti, M. J. 2013, Optics Express, 21, 404, aDS Bibcode: 2013OExpr..21..404K
- Lacour, S., Nowak, M., Wang, J., et al. 2019, Astronomy & Astrophysics, 623, L11
- Lafrenière, D., Marois, C., Doyon, R., & Barman, T. 2009, The Astrophysical Journal, 694, L148
- Lagrange, A.-M. 2014, Philosophical Transactions of the Royal Society A: Mathematical, Physical and Engineering Sciences, 372, 20130090
- Lagrange, A.-M., Bonnefoy, M., Chauvin, G., et al. 2010, Science, 329, 57
- Lavvas, P. & Arfaux, A. 2021, Monthly Notices of the Royal Astronomical Society, 502, 5643
- Lee, J.-M., Heng, K., & Irwin, P. G. 2013, The Astrophysical Journal, 778, 97
- Lyot, B. 1939, MNRAS, 99, 580
- Macintosh, B. 2021, HEDS | Direct Imaging of Extrasolar Planets, high Energy Density Science Seminar Series, LLNL-VIDEO-825119, Livermore Lab, <https://youtu.be/tGcjcPhgvEM>, last access 2023-03-30
- Macintosh, B., Graham, J., Barman, T., et al. 2015, Science, 350, 64
- Macintosh, B., Graham, J. R., Ingraham, P., et al. 2014, Proceedings of the National Academy of Sciences, 111, 12661, publisher: Proceedings of the National Academy of Sciences
- Madhusudhan, N. 2012, The Astrophysical Journal, 758, 36
- Madhusudhan, N. 2019, Annual Review of Astronomy and Astrophysics, 57, 617
- Mansuripur, M. 2002, Classical optics and its applications (Cambridge University Press)
- Marley, M. S., Ackerman, A. S., Cuzzi, J. N., & Kitzmann, D. 2013, Comparative climatology of terrestrial planets, 1, 367
- Marois, C., Lafreniere, D., Doyon, R., Macintosh, B., & Nadeau, D. 2006, The Astrophysical Journal, 641, 556
- Marois, C., Macintosh, B., Barman, T., et al. 2008, science, 322, 1348
- Marois, C., Macintosh, B., & Véran, J.-P. 2010a, in Adaptive Optics Systems II, Vol. 7736, SPIE, 595–606
- Marois, C., Zuckerman, B., Konopacky, Q. M., Macintosh, B., & Barman, T. 2010b, Nature, 468, 1080
- Marquez-Neila, P., Fisher, C., Sznitman, R., & Heng, K. 2018, Supervised Machine Learning for Analysing Spectra of Exoplanetary Atmospheres
- Mendonça, J. M., Tsai, S.-m., Malik, M., Grimm, S. L., & Heng, K. 2018, The Astrophysical Journal, 869, 107
- Menou, K. 2019, Monthly Notices of the Royal Astronomical Society: Letters, 485, L98
- Meru, F., Rosotti, G. P., Booth, R. A., Nazari, P., & Clarke, C. J. 2019, Monthly Notices of the Royal Astronomical Society, 482, 3678
- Michel Mayor, D. Q. 1995, Nature, 378, 355
- Miles, B. E., Biller, B. A., Patapis, P., et al. 2022, arXiv preprint arXiv:2209.00620
- Miles, B. E., Biller, B. A., Patapis, P., et al. 2023, The Astrophysical Journal Letters, 946, L6
- Miles, B. E., Skemer, A. J., Barman, T. S., Allers, K. N., & Stone, J. M. 2018, The Astrophysical Journal, 869, 18
- Millar-Blanchaer, M. A., Girard, J. H., Karalidi, T., et al. 2020, The Astrophysical Journal, 894, 42
- Miret-Roig, N. 2023, Astrophysics and Space Science, 368, 17
- Molliere, P. 2021, Measuring and interpreting the abundances of exoplanet atmospheres, iAP weekly specialised seminars, Institut d'Astrophysique de Paris, <https://youtu.be/oKNU7wD4sZo>, last access 2023-03-30
- Mollière, P., Molyarova, T., Bitsch, B., et al. 2022, The Astrophysical Journal, 934, 74
- Mollière, P., Stolkér, T., Lacour, S., et al. 2020, Astronomy & Astrophysics, 640, A131
- Morley, C. V., Marley, M. S., Fortney, J. J., et al. 2014, The Astrophysical Journal, 787, 78
- Moses, J. I., Marley, M. S., Zahnle, K., et al. 2016, The Astrophysical Journal, 829, 66
- NASA, M. 2023, 2M1207 b - First image of an exoplanet
- NASA Exoplanet Archive. 2023, Planetary Systems, *NExSci-Caltech/IPAC*. <https://catcopy.ipac.caltech.edu/dois/doi.php?id=10.26133/NEA12>, Version: 2023-03-27 12:00. DOI: [10.26133/NEA12](https://doi.org/10.26133/NEA12)
- NASA Exoplanet Exploration Program. 2023, <https://exoplanets.nasa.gov/discovery/exoplanet-catalog/>, [Online; accessed 31-March-2023]
- Nguyen, M. M., De Rosa, R. J., & Kalas, P. 2020, The Astronomical Journal, 161, 22
- Nowak, M., Lacour, S., Lagrange, A.-M., et al. 2020a, Astronomy & Astrophysics, 642, L2
- Nowak, M., Lacour, S., Mollière, P., et al. 2020b, Astronomy & Astrophysics, 633, A110
- Öberg, K. I. & Bergin, E. A. 2021, Physics Reports, 893, 1
- Palma-Bifani, P., Chauvin, G., Bonnefoy, M., et al. 2022, arXiv preprint arXiv:2211.01474
- Patapis, P., Nasedkin, E., Cugno, G., et al. 2022, Astronomy & Astrophysics, 658, A72
- Pérez, S., Casassus, S., Baruteau, C., et al. 2019, The Astronomical Journal, 158, 15
- Perryman, M., Hartman, J., Bakos, G. A., & Lindegren, L. 2014, The Astrophysical Journal, 797, 14
- Petrus, S., Bonnefoy, M., Chauvin, G., et al. 2021, Astronomy & Astrophysics, 648, A59
- Petrus, S., Chauvin, G., Bonnefoy, M., et al. 2023, Astronomy & Astrophysics, 670, L9
- Pinte, C., Hammond, I., Price, D. J., et al. 2023, Monthly Notices of the Royal Astronomical Society: Letters, slad010
- Polman, J., Waters, L., Min, M., Miguel, Y., & Khorshid, N. 2022, arXiv preprint arXiv:2208.00469
- Rimmer, P., Helling, C., & Bilger, C. 2014, International Journal of Astrobiology, 13, 173
- Rodet, L. & Lai, D. 2022, Monthly Notices of the Royal Astronomical Society, 516, 5544
- Ruffio, J.-B., Horstman, K., Mawet, D., et al. 2023, arXiv preprint arXiv:2301.04206
- Ruffio, J.-B., Konopacky, Q. M., Barman, T., et al. 2021, The Astronomical Journal, 162, 290
- Sahlmann, J., Lazorenko, P., Ségransan, D., et al. 2016, Astronomy & Astrophysics, 595, A77
- Sengupta, S. & Marley, M. S. 2016, The Astrophysical Journal, 824, 76
- Showman, A. P. & Kaspi, Y. 2013, The Astrophysical Journal, 776, 85
- Sing, D. K., Fortney, J. J., Nikolov, N., et al. 2016, Nature, 529, 59
- Skemer, A. J., Marley, M. S., Hinz, P. M., et al. 2014, The Astrophysical Journal, 792, 17
- Skemer, A. J., Morley, C. V., Zimmerman, N. T., et al. 2016, The Astrophysical Journal, 817, 166
- Smith, W. H. 1987, Publications of the Astronomical Society of the Pacific, 99, 1344
- Snik, F., Otten, G., Kenworthy, M., Mawet, D., & Escuti, M. 2014, in, 91477U
- Stevenson, K. B., Bean, J. L., Fabrycky, D., & Kreidberg, L. 2014, The Astrophysical Journal, 796, 32
- Stolkér, T., Min, M., Stam, D. M., et al. 2017, Astronomy & Astrophysics, 607, A42
- Stone, J. M., Skemer, A. J., Kratter, K. M., et al. 2016, The Astrophysical Journal Letters, 818, L12
- Sullivan, P. W., Winn, J. N., Berta-Thompson, Z. K., et al. 2015, ApJ, 809, 77
- Suttliff, B. J., Birkby, J. L., Stone, J. M., et al. 2023, Monthly Notices of the Royal Astronomical Society, 520, 4235, aDS Bibcode: 2023MNRAS.520.4235S
- Tan, X. & Showman, A. P. 2021, Monthly Notices of the Royal Astronomical Society, 502, 678
- Thompson, S. E., Coughlin, J. L., Hoffman, K., et al. 2018, The Astrophysical Journal Supplement Series, 235, 38
- van Holstein, R. 2021, Phd thesis, Leiden University, Leiden Observatory, <https://hdl.handle.net/1887/3217115>, version 2023-03-28
- Van Holstein, R. & Stam, D. 2016, Masters thesis, Delft University of Technology, Faculty of Aerospace Engineering, Space Engineering Department, <http://resolver.tudelft.nl/uuid:56dd5ce4-c68f-4145-a328-0d8054591ae1>, version 2023-03-28
- Van Holstein, R. G., Snik, F., Girard, J. H., et al. 2017, in Techniques and Instrumentation for Detection of Exoplanets VIII, Vol. 10400, SPIE, 315–330
- Vigan, A., Moutou, C., Langlois, M., et al. 2010, Monthly Notices of the Royal Astronomical Society, 407, 71
- Wagner, K., Apai, D., Kasper, M., McClure, M., & Robberto, M. 2022, The Astronomical Journal, 163, 80
- Wang, J., Wang, J. J., Ma, B., et al. 2020, The Astronomical Journal, 160, 150
- Wang, J., Wang, J. J., Ruffio, J.-B., et al. 2022, The Astronomical Journal, 165, 4
- Wang, J. J., Ruffio, J.-B., Morris, E., et al. 2021, The Astronomical Journal, 162, 148
- Welzel, L. 2021, Effect of planet migration on dust rings, part of *Star and Planet Formation* course of 2021. Lecturer Melissa McClure, Leiden Observatory, Leiden University. Unpublished course essay. Online: [Effect of planet migration on dust rings](#).
- Whiteford, N., Glasse, A., Chubb, K. L., et al. 2023, arXiv preprint arXiv:2302.07939
- Woitke, P., Herbst, O., Helling, C., et al. 2021, Astronomy & Astrophysics, 646, A43
- Zhang, Y., Ginski, C., Huang, J., et al. 2023, arXiv preprint arXiv:2302.12824
- Zhang, Y., Snellen, I. A., Bohn, A. J., et al. 2021, Nature, 595, 370
- Zhou, Y., Bowler, B. P., Apai, D., et al. 2022, The Astronomical Journal, 164, 239
- Zugger, M. E., Kasting, J. F., Williams, D. M., Kane, T. J., & Philbrick, C. R. 2010, The Astrophysical Journal, 723, 1168

Appendix A: Data

This research has made use of the NASA Exoplanet Archive, which is operated by the California Institute of Technology, under contract with the National Aeronautics and Space Administration under the Exoplanet Exploration Program.

Appendix B: Plotting

All original plots in this work were produced by Lukas Welzel and can be reproduced using the repository at https://github.com/lwelzel/exoplanets_a-direct-imaging.git. To reproduce the general exoplanet corner plot obtain the data from the [NASA Exoplanet Archive \(2023\)](#), either as pre-filtered or raw table data. The data required to reproduce the C/O ratio plot is included in the repository and built to complement/extend the online table by [Currie et al. \(2022a\)](#) at <https://tinyurl.com/srb33b>.

Work Distribution

Table B.1. Contributor information.

Name	Student number
L. Welzel	s3079449
R. van Gaalen	s2351854
J.A. Barendse	s1715445
O.B. Swida	s3405125

Signatures:

L. Welzel

R. van Gaalen

J.A. Barendse

O.B. Swida

Authors are ordered by contribution in the following, from large to small.

1	Introduction: Okta	1
2	Methods	2
2.1	Instruments: Remon	2
2.2	Polarimetry: Lukas	3
2.3	Astrometry: Lukas	3
2.4	Disk Kinematics & Dust Trapping: Lukas	3
2.5	Differential Imaging: Lukas	3
2.6	Molecular Mapping: Lukas	4
2.7	Modeling: Remon	4
2.8	Verification & Characterization: Okta	4
3	Results	5
3.1	Population: Joost	5
3.2	Atmospheres: Lukas	5
3.3	Examples: Joost	8
3.4	Far-Out, High Eccentricity or Free Floating Planets?: Lukas	9
4	Discussion	9
4.1	Atmospheres: Lukas	9
4.2	Planet & Star Formation: Lukas	9
4.3	Limits & Bias: Okta, Remon, Lukas (only T-R-cloud deg.)	9
4.4	Future Instruments: Remon	9
5	Conclusion: Okta, Lukas	10
A	Data: Lukas	12
B	Plotting: Lukas	12